in International Research on Thermodynamic and Transport Properties," p. 687, Academic Press, New York (1962).
7. White, J. L., and A. B. Metzner, *A.I.Ch.E. J.*, 11, 324 (1965).
8. Birkoff, G., "Hydrodynamics," 2 ed., Princeton Univ. Press, N. J. (1960).
9. Michal, A. D., *Proc. Natl. Acad. Sci.*, 37, 623 (1951).
10. Morgan, A. J. A., *Quart. J. Math.*, 3, No. 2, 250 (1952).
11. Ames, W. F., "Nonlinear Partial Differential Equations," Academic Press, New York (1965).
12. ———, *Ind. Eng. Chem. Fundamentals*, 4, 72 (February, 1965).
13. Hansen, A. G., "Similarity Analysis of Boundary Value Problems in Engineering," Prentice-Hall, Englewood Cliffs, N. J. (1964).
14. Schlichting, Hermann, "Boundary Layer Theory," Pergamon Press, New York (1955).
15. Shah, M. J., Ph.D. dissertation, Univ. California, Berkeley (1959).
16. Goldstein, S., *Proc. Camb. Phil. Soc.*, 35, 338 (1939).
17. Sparrow, E. M., and J. L. Gregg, *Trans. Am. Soc. Mech. Engrs.*, 80, 379 (1958).
18. Klamkin, M. S., *SIAM Rev.*, 4, 1, 43 (1963).
19. Davis, H. D., "Introduction to Nonlinear Differential and Integral Equations," Dover Publication (1962).

Manuscript received November 9, 1965; revision received January 31, 1966; paper accepted February 1, 1966.

Entrainment of Air into a Liquid Spray

FRANCIS E. J. BRIFFA and NORMAN DOMBROWSKI

Imperial College, London, England

An investigation has been carried out into the flow pattern existing in and around a flat spray, particular attention being paid to the region of disintegration of the liquid sheet. The mass of air entrained into the spray, the decay of air velocity along the spray axis, and the spread of the drops in the plane normal to that of the sheet have been related to the operating conditions by equations theoretically derived and experimentally confirmed. Similarities between the characteristics of air entrainment into liquid sprays and into gas jets have been noted.

A spray nozzle is a device which transforms bulk liquid into a spray and which projects the spray in a controlled direction. While many studies have been made of the processes of drop formation, little attention has been given to the subsequent history of the resulting spray and to the way in which it interacts with the surrounding atmosphere.

The aerodynamic properties of sprays are significant in a wide range of applications; for example, in a spray dryer the initial rate of mixing of the spray with the hot gas plays a large part in determining the bulk density of the final dried product. In a combustion chamber the burning characteristics of a fuel spray depends on both the manner in which the air is entrained and mixes with the spray, and on the final mixture ratio. Furthermore, the penetration of the fuel drops through the hot gases will depend inter alia on the induced gas stream carrying them along.

Previous investigations (*1* to *3*) have been concerned with the entrainment of air into sprays produced from hollow-cone and solid-cone swirl spray nozzles. However, the complex nature of these systems has presented a series of experimental and theoretical difficulties and there are still a number of features about the processes of momentum transfer within a moving cloud of drops which remain to be elucidated.

In order to obtain a clearer picture of the detailed mechanism of air entrainment we have studied a flat spray, since this simplifies both the experimental and theoretical approach. Fan spray nozzles were utilized for this research because of the considerable information available on their characteristics (*4* to *11*).

Francis E. J. Briffa is with Shell Research, Ltd., Egham, Surrey, England. Norman Dombrowski is at the University of Leeds, Leeds, England.

EXPERIMENTAL PROCEDURE

The factors which may be expected to affect the entrainment of air by a liquid spray are: the density and vapor pressure of the liquid; the spray velocity; drop size and size distribution; the liquid volume flow rate; the density and viscosity of the ambient gas stream; and ambient gas velocity. In the present research most of the experiments were carried out with a single liquid, while air at room temperature only was used as the ambient gas.

Apparatus

The experiments were carried out in a vertical 1-ft. × 1-ft., 6-in. rectangular air duct as shown in Figure 1. The entrance section was designed (*12*) to insure fully developed flow at the end of the contraction, while flow straighteners, 2½ in. long × ¼ in. wide, were inserted at the beginning of the parallel section. Three of the walls of the duct were fitted with twin-ground plate glass windows, while the interior of the fourth had a black nonreflecting surface.

The nozzle was mounted at the top of a vertical feed pipe to spray vertically upward, the liquid being introduced into the pipe by means of a tube placed across the duct below the flow straighteners. Test liquid was contained in a pressure vessel and ejected through the nozzle by means of compressed nitrogen, the nozzle being positioned such that the plane of the sheet was parallel to the two opposite windows. Air was drawn up through the duct past the nozzle by a centrifugal fan.

Cameras and associated optical and lighting equipment were mounted on an adjustable platform which could be placed at any height above the spray nozzle.

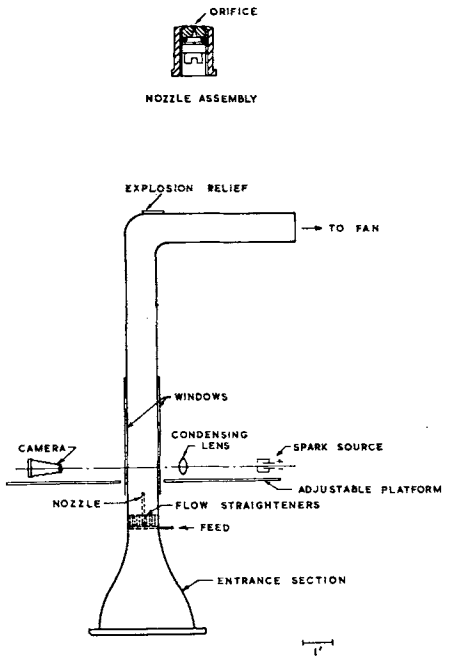

Fig. 1. General layout of apparatus.

Measurement of Air Velocity

The velocity of the air drawn into the spray was determined by viewing the side of the spray and by measuring the velocity of lycopodium particles suspended in the air stream. The latter was carried out by taking double microsecond flash photographs of the particles on the same plate and by measuring the distance moved by each particle in a known interval of time. Lycopodium powder was selected because of its uniform size (28.8 microns) and small settling velocity (*13*) (1.71 cm./sec.). The particles were introduced some 6 in. below the nozzle. Since the leading edge of the sheet is convex to the orifice (see Figure 2), the profile along the spray axis tends to be masked by the profile along the edge of the spray. In order to photograph the particles entering the spray, the spray sheet was rotated about its axis approximately 5 deg. so that its boundary was off-set from the optical axis. Individual lycopodium particles could not be identified within the spray. However, it can be shown that drops of the order of 15 microns in diameter move with a velocity very close to that of the air stream, and the air velocity within the spray was taken to be equal to the velocity of these drops. In this study the air velocity within the spray has been determined only along the spray axis in the plane of the spray sheet.

Physical Properties of Liquids Employed

All of the work has been carried out with iso-octane, apart from a few experiments with tetralin (1.2.3.4-tetrahydronaphthalene). Their physical properties are given in Table 1.

Drop-Size Relations of Spray Nozzles

Delavan-Watson 5L single-hole fan spray nozzles similar to those described previously (*6*) were employed in these experiments. Details are given in Table 2, the parameter K_o in the last column being a function of the orifice area. Nozzle 5LA was used with iso-octane, while 5LB was used with tetralin.

Table 1. Properties of Liquids at 60°F. (*14*)

Liquid	Iso-octane	Tetralin
Density, g./cc.	0.69	0.97
Surface tension, dynes/cm.	18.90	36.00
Viscosity, centipoise	0.54	2.00

A wide range of techniques may be employed to measure the drop size of sprays. This research has been principally concerned with the entrainment characteristics of the sprays in the vicinity of the nozzle, and since Hasson and Mizrahi (*8*) have shown that the size may vary with distance from the nozzle as a result of coalescence, a photographic technique was chosen because it could be used to examine the spray close to the nozzle where the drops move at their highest velocity (circa 4,500 cm./sec.). The method consisted of taking submicrosecond flash photographs of the spray near the region of disintegration and counting and sizing the drops from the resulting negatives. The results have been expressed in terms of the number mean diameter and correlated with the operating variables by

$$d_{10} = 132 \left(\frac{K_o \gamma}{\Delta P} \right)^{1/3} \left(\frac{\rho_1}{\rho_a} \right)^{1/6} \pm 2.8 \text{ microns} \quad (1)$$

Drop-size measurements were carried out at a duct air velocity of 23 cm./sec. Equation (1), expressed in terms of relative liquid sheet-air velocity, predicts increases of drop sizes ranging from about 10% at the lowest ejection pressure to 3% at the highest pressure as the air velocity is increased to 155 cm./sec., the maximum used in this research. A few experiments were therefore carried out at the highest duct velocity to confirm this point. However, no effect on drop size could be detected. This result is likely to be due to the fact that the air velocity adjacent to the spray sheet, particularly near its root, was less than the free stream velocity as a consequence of partial shielding by the nozzle assembly.

The results have also been expressed as a function of the surface-volume mean diameter for comparison with previous work (*9*) where drop sizes from larger nozzles have been similarly measured and expressed in terms of this diameter. In this case, the value of the constant is 230, which compares favorably with the previously found value of 236.

In order to detect whether any changes in the size spectrum occurred as the spray moved away from the nozzle as a result of subsequent drop coalescence or evaporation, further measurements of drop size were carried out at an ejection pressure of 118 lb./sq.in. The drag experienced by a drop is a function of its diameter; consequently the drop velocity spectrum, and hence the spatial size distribution, will vary during the passage of the spray through the atmosphere. In order to avoid a tedious analysis involving the determination of both the size and velocity spectra, measurements were made only at a height of 12 cm. above the nozzle where double-flash photographs revealed that drop velocities were sensibly uniform. The experiments showed that at this distance the drop size remained effectively constant and thus indicated the absence of any appreciable drop coalescence or evaporation.

Range of Experiments and Procedure

Experiments were carried out with iso-octane at air velocities of 23, 72, 105, and 155 cm./sec. and differential ejection pressures of 7.6, 22.5, 45.5, 76.8, and 118 lb./sq.in., the intervals being selected to provide equal velocity increments. For tetralin tests were carried out with differential pressures

Table 2. Dimensions of Nozzles

Nozzle	Orifice dimensions, cm.	Orifice area, sq. cm.	Flow No. $\left(\frac{\text{imperial gal./hr}}{\sqrt{\text{lb./sq. in.}}}\right)$	Discharge coefficient, C_q	Nozzle parameter (*6*) K_o, sq. cm.
5LA	0.0228 × 0.0349	0.000797	0.27 (iso-octane)	0.95	5×10^{-4}
5LB	0.0197 × 0.0331	0.000653	0.21 (tetralin)	0.91	3.2×10^{-4}

of 45.5, 76.8, and 118 lb./sq.in. at a single air velocity of 58 cm./sec.

For each ejection pressure double-flash photographs were taken of the spray to determine the velocity of 15-micron diameter drops in the plane of the liquid sheet along the axis at 6.6, 9.6, and 12 cm. from the nozzle. Air velocities were measured at 0.1-cm. intervals above the nozzle, at each level the data were recorded at the air-spray interface and at 1-cm. intervals from the plane of the sheet, up to a distance of 3 cm.

Single-flash photographs were also taken of the side of the spray in order to determine its depth across the axis.

The lengths of the coherent liquid sheets have been measured from flash photographs of the sprays with an accuracy of approximately 1 wavelength, which for the longest sheets is of the order of 0.2 cm.

BOUNDARY OF THE SPRAY

Figure 2 is a typical photograph of a sheet disintegrating through aerodynamic action. Rapidly growing waves are produced on the sheet which subsequently break down at the crests. Fragments of sheet then rapidly contract into ligaments which break down into drops. A number of drops are also produced at the point of fragmentation; these drops have an additional velocity component resulting from the accelerating wave crest and thus the initial depth of the spray is greater than the amplitude of the waves.

Figure 3 illustrates the boundary of a spray, which is defined here by the region of disintegration and the width and depth of the spray at any given point. The break-up length of the sheet depends upon the liquid properties and operating conditions. The width of the spray at the region of disintegration is determined by the extent to which the side edges of the liquid sheet have contracted by surface tension (6); beyond the region of disintegration, the edges of the spray are principally determined by those drops which sustain the direction of flow of the edge of the sheet at disintegration. At low air densities (9) or low air-liquid relative velocities (7), the majority of the spray may result from drops produced from the sheet edge. At atmospheric pressure, particularly for liquids of low surface tension at high differential ejection pressures, these drops generally constitute only a small proportion of the total mass flow rate. However, in order to insure that measurements corresponded to known liquid flow rates, all measurements were confined to a sector of 5 deg. included angle around the spray axis in the plane of the sheet. In vacuum a spray diverges from its source. However in a cocurrent air stream the path of the drops tends toward that of the air. It is shown below that induced air velocities within the sprays are generally much higher than those of the surrounding air stream so that the drops approximate to their original paths. The depth of the spray is determined by the trajectories of the fine drops thrown out of the plane of the sheet. In this region induced air streams have relatively low velocities and the direction of the drops is considerably influenced by the adjacent air.

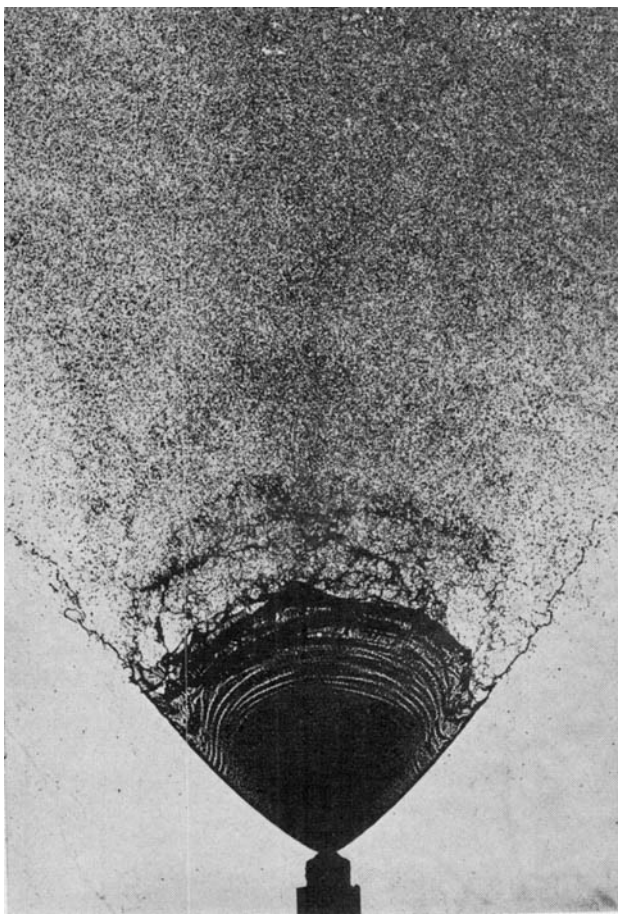

Fig. 2. Disintegration of sheet.

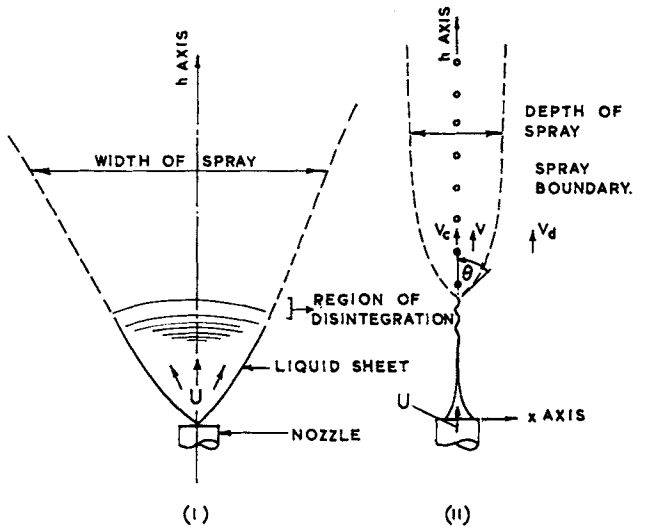

Fig. 3. Spray boundary.

Length of the Coherent Liquid Sheet

A theoretical relation for the coherent length of a liquid sheet has been derived by Dombrowski and Hooper (9) on the basis of a theory presented by Squire (15), and it was shown that at atmospheric density

$$r_t^{*2} = \frac{3}{2}\,\frac{\rho_l}{\rho_a} K_o\; E\; N_{We}^{1/2}\,\frac{(N_{We}+1)}{(N_{We}-1)^2} \qquad (2)$$

In the present work, apart from experiments carried out at the lowest ejection pressure, N_{We} was found to be greater than 20. Under these conditions Equation (2) may be simplified to give

$$r_t^* = 4.5\left[\frac{E^2\gamma\,\rho_l\,K_o}{\rho_a^2\,U^2}\right]^{1/3} \qquad (3)$$

By utilizing Equation (3) the measured lengths of the coherent liquid sheet were linearly correlated with the operating variables by

$$r_m^* = 1{,}990\left[\frac{\gamma\,\rho_l\,K_o}{U^2}\right]^{1/3} - 0.51 \pm 0.24 \qquad (4)$$

Depth of Spray

A fan spray has a finite depth because drops are produced in the region of disintegration which have a velocity component derived from that of the wave amplitude.

The amplitude of a wave is given by (11)

$$x' = x_o \exp(\alpha t^{3/2}) \tag{5}$$

Differentiating Equation (5) one obtains

$$\frac{dx'}{dt} = \frac{3}{2}\alpha t^{3/2}\frac{x'}{t} \tag{6}$$

At break-up, $x' = x^*$, and $t = t^* = r^*/U$; hence combining Equations (5) and (6) one obtains dx'/dt at break-up, that is

$$\left(\frac{dx'}{dt}\right)^* = \frac{3E}{2}\frac{U}{r^*}x^* \tag{7}$$

No measurements were made of the value of x^* and of the manner in which it varied with the operating variables. However, if it is assumed that x^* is a function of U/r^* over a limited range of conditions, then by taking E to be constant (9) Equation (7) may be rewritten as

$$\left(\frac{dx'}{dt}\right)^* = f\left(\frac{U}{r^*}\right) \tag{8}$$

The initial normal velocity component of the drops can be expected to be a function of $(dx'/dt)^*$; hence we may write

$$u_n = f'(U/r^*) \tag{9}$$

where u_n is given by $u_n = u_r \tan\theta$, and u_r the initial radial velocity component of a drop, that is, the velocity along planes parallel to that of the sheet, and in the direction of the radial streamlines of the sheet, is given approximately by (6)

$$u_r = C_q\sqrt{\frac{2\Delta P}{\rho_l}} \tag{10}$$

Values of u_n were plotted against U/r^*, r^* values being obtained from Equation (4), and it was found the results could be linearly correlated by

$$u_n = 0.084\ U/r^* + 1{,}530 \pm 105 \tag{11}$$

Trajectory of Drop at Air Spray Interface

By assuming a Stokes flow regime, the equation of motion for any drop traveling along the edge of the spray and moving vertically upward can be shown to be (16)

$$h = \frac{1}{B}[\{U + (g/B - v_d)\}\{1 - e^{-Bt}\} - (g - v_dB)t] + r^* \tag{12}$$

The initial horizontal, or normal, velocity component of a given drop depends upon its position in space at the time of its formation. The velocity component at the instant of break-down will be greatest for a drop formed at a wave crest, while it will be zero on the spray axis. The equation of motion in the horizontal direction may therefore be written as

$$x = \frac{C}{B}u_n(1 - e^{-Bt}) \tag{13}$$

where C has any value from 0 to 1, depending upon the initial position of the drop in the wave.

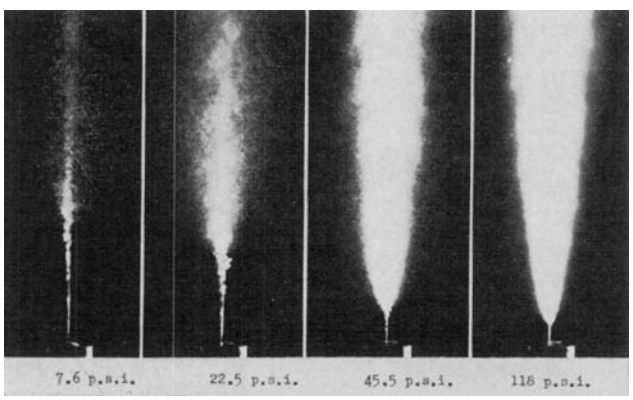

Fig. 4. Profile of spray at various ejection pressures.

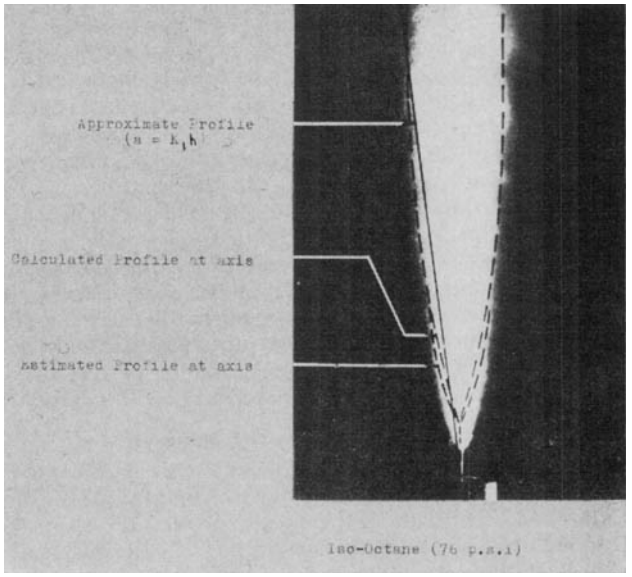

Fig. 5. Superimposition of calculated and observed spray profiles.

Figure 4 shows photographs of the edge of a spray viewed along the plane of the sheet. The photographs indicate that drop concentration decreases with distance from the plane so that the edge of the spray is indistinct. However, on each side there is a region where the drop concentration rapidly diminishes and this boundary has been taken as the effective profile of the spray. It is likely that the liquid distribution depends principally on the mechanism of sheet disintegration and thus for a particular mechanism, for example, aerodynamic wave formation, it could be expected to vary little with operating conditions. Consequently, C will be a measure of the fractional liquid concentration across the spray and thus the effective edge of the spray, as chosen from the region of greatest change of density on the photographic negative, corresponds to a constant value of C.

In the present study no attempt was made to measure the variation in drop size across the spray, and Equations (12) and (13) were utilized by drawing a series of curves for a range of values of d and C. It was found that, except for the differential ejection pressure of 7.6 lb./sq.in., where the profile was too diffuse for accurate identification, good agreement between calculated and measured spray profiles was obtained when the drop diameter was equal to $1.3 \times d_{10}$ and when $C = 0.4$. It is of interest to note that for each experiment the effective diameter is equivalent to the surface-mean diameter of the whole spray.

Although the profile along the spray axis is masked by the profile along the edge of the spray, the actual profile along the axis can easily be estimated from the geometry of the system. This is drawn in Figure 5, which also shows the profile as calculated from Equations (12) and (13).

The photographs in Figure 4 also indicate that as the ejection pressure is raised, the break-up length decreases, the spray becomes finer, and the boundary becomes more distinct. Comparison of the depths of the sprays shows the rate of spread tends to be linear as the ejection pressure is increased.

MASS RATE OF AIR ENTRAINMENT INTO SPRAY

When a spray moves through a gas it experiences aerodynamic drag and because momentum is conserved within the system, the reduction of drop velocity is accompanied by an increase in the local gas velocity. Since this results in a forward displacement of the gas, an equivalent mass of gas flows (or is entrained) into the spray.

An exact analysis of the momentum transfer from a decelerating spray to the surrounding air stream requires a detailed knowledge of the nature of the flow fields around each drop and of the manner in which interacting fields affect the movement of the drops. In this study a simple theoretical model has been set up and analyzed, and it has been found that the salient features of the air spray system may be satisfactorily described on this basis.

Air Velocity Distribution Across the Spray

It is assumed in the following analysis that the air velocity distribution is determined primarily by the liquid flowing in the plane of the sheet, and that the shear stress experienced at the air spray interface in the plane of the sheet is similar to that produced by turbulent flow past a flat solid surface.

When a fluid such as air flows under turbulent conditions it may be shown from Prandtl's mixing length theory (*17*) that the velocity distribution normal to the surface is given by

$$\sqrt{\frac{R}{\rho_a}}\,\frac{\ln x}{\delta} = -v + \text{constant} \qquad (14)$$

If we assume that the analogous plate at the center of the spray has protuberances with a characteristic dimension d_o such that when $x = d_o$, $v = v_c - v_d$, then

$$v = v_c - v_d - \frac{\sqrt{R/\rho_a}}{\delta}\ln\frac{x}{d_o} \qquad (15)$$

The shear stress at a surface is represented by

$$R = \rho_a\,(v_c - v_d)^2\,K^2 \qquad (16)$$

Hence from Equations (15) and (16)

$$v = v_c - v_d - \frac{(v_c - v_d)}{\beta}\ln\frac{x}{d_o} \qquad (17)$$

where

$$\beta = \delta/K \qquad (18)$$

According to Schlichting (*18*), K^2 is independent of the surface roughness and is given by

$$K^2 = 0.5\left(2\log\left[\frac{U_p\,l\,\rho_a}{\mu}\right] - 0.65\right)^{-2.3} \qquad (19)$$

provided e, the height of a protuberance on the surface, is less than $(100\,\mu)/(\rho_a\,U_p)$. Critical values of e for sprays (e_{crit}) have been evaluated by taking U_p to represent the average difference between the air velocity along the spray axis and the duct air velocity. The values are listed in Table 3 and it is seen that they are at least four times as great as the number mean diameter. Equation (19) cannot be strictly applied to sprays, since for plates U_p remains constant with increase of l, while that for sprays decreases. However, because of the logarithmic form of the relation, the value of K^2 is not very sensitive to changes in the product $U_p l$ and it should provide a reasonable estimate of K^2 for sprays.

TABLE 3. AIR FLOW CHARACTERISTICS OF SPRAYS (ISO-OCTANE DUCT VELOCITY v_d OF 105 CM./SEC.)

Differential ejection pressure ΔP, lb./sq. in.	Height above nozzle h, cm.	Mean drop size d_{10}, microns	e_{crit}, microns	K^2 [Equation (29)]	β, δ/K	Vertical component of air velocity at boundary of spray v, cm./sec.	Air velocity along spray axis v_c, cm./sec.	$\frac{v_c - v_d - v}{v_c - v_d}$	Distance of boundary from axis a, cm.	d_o, microns
7.6	($r^* = 2.9$)	40	430	—	—	—	—	—	—	—
	4			0.0066	5.0	8	590	0.98	0.6	40
	6			0.0062	5.1	−1	350	1.01	0.9	48
	8			0.0064	5.0	0	240	1.00	1.0	96
	10			0.0064	5.0	0	200	1.00	1.1	84
22.5	($r^* = 1.7$)	28	226	—	—	—	—	—	—	—
	4			0.0048	5.8	4	930	1.00	1.0	28
	6			0.0048	5.8	4	580	0.99	1.0	28
	8			0.0045	6.0	−10	400	1.03	1.0	22
	10			0.0048	5.8	6	340	0.98	1.1	31
45.5	($r^* = 1.3$)	22	121	—	—	—	—	—	—	—
	2			0.0050	5.6	5	2,340	1.00	0.6	22
	4			0.0039	6.5	30	1,660	0.98	0.9	17
	6			0.0038	6.5	5	1,140	1.00	1.0	20
	8			0.0039	6.5	15	750	0.98	1.0	20
	10			0.0042	6.2	15	510	0.96	1.1	22
76.8	($r^* = 1.1$)	19	80	—	—	—	—	—	—	—
	2			0.0044	6.1	0	3,180	1.00	0.5	11
	4			0.0035	6.8	15	2,500	1.00	0.8	10
	6			0.0034	6.8	25	1,920	0.99	1.0	10
	8			0.0033	6.9	10	1,400	0.99	1.0	10
	10			0.0035	6.8	20	910	0.98	1.2	13
118	($r^* = 0.8$)	16	66	—	—	—	—	—	—	—
	2			0.0035	6.8	−3	3,780	1.00	0.5	6
	4			0.0033	7.0	16	2,940	0.99	0.7	6
	6			0.0032	7.1	27	2,260	0.99	1.0	8
	8			0.0031	7.1	10	1,700	1.00	1.0	6
	10			0.0032	7.1	18	1,220	0.99	1.2	10

Calculated values of K^2 are listed in Table 3, together with corresponding values of β, taking the value of $\delta = 0.4$ for air. It can be noted that for a given ejection pressure β remains approximately constant along each spray and that ejection velocity has only a small effect.

Values of the vertical velocity component of the air stream at the spray boundary together with corresponding axial velocities are listed in columns 6 and 7. Values of $(v_c - v_d - v)/(v_c - v_d)$ at the spray boundary are listed in column 8 and are seen to be close to unity. Thus from Equation (17), d_o is given by

$$d_o = a\, e^{-\beta} \tag{20}$$

and has values little affected by duct velocity as shown in the last column of Table 3. The figures show that, apart from the lowest pressure where measurements of a are least accurate, d_o tends to be equal to or less than d_{10}, the difference increasing with increase of pressure. While at this stage no conclusions can be drawn regarding the significance of the comparison, it should be noted that the measured values of d_{10} are greater than those actually existing within the sprays, since the photographic technique did not permit drops smaller than 15 microns in diameter to be resolved. Since the number of small drops increases with increasing pressure, it is likely that the divergences between d_{10} and d_o at the higher pressures are less than indicated.

Figure 6 shows typical examples of the air flow pattern within and around sprays for duct air velocities of 23 and 105 cm./sec. The arrows indicate the direction of the local air flow, while the adjacent figures denote the velocity in centimeters per second. It will be noted that for a given duct air velocity, the magnitude and inclination of air velocity to the boundary increase with ejection pressure and with proximity to the region of disintegration. Equation (17) is plotted in Figure 7 for a differential ejection pressure of 45.5 lb./sq.in. and a duct air velocity of 105 cm./sec. to show the nature of the theoretical velocity profiles across the spray at various heights above the nozzle axis. In practice it would be expected that because of the spread of the drops, the velocity gradient close to the spray axis would be less than that indicated on the figure.

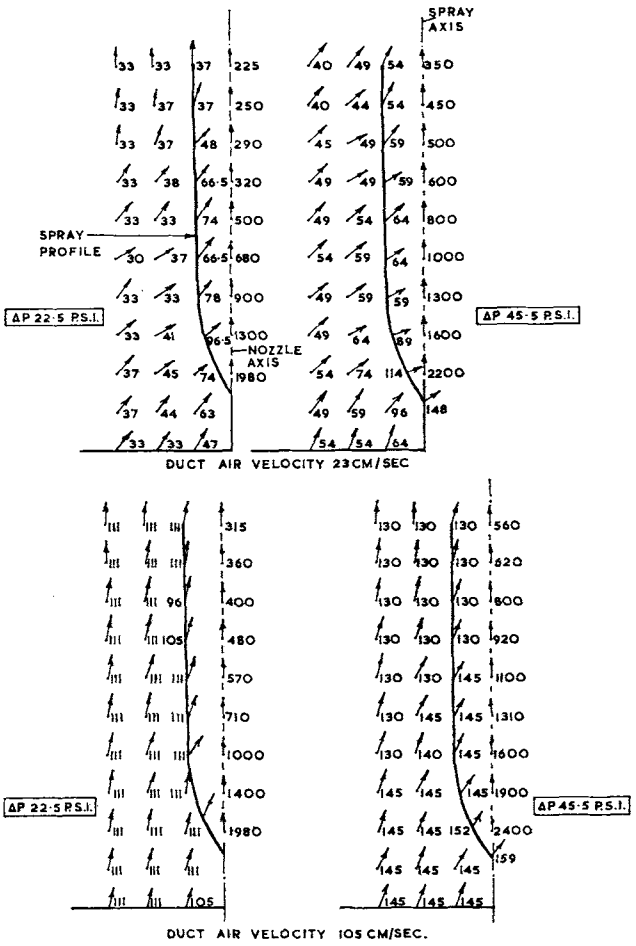

Fig. 6. Air flow pattern around spray.

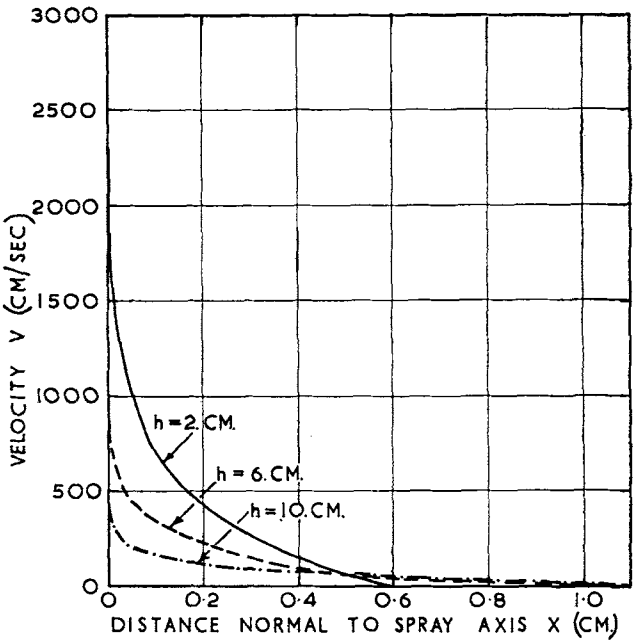

Fig. 7. Velocity profile across spray at various heights above nozzle. $\Delta P = 45.5$ lb./sq.in. $v_d = 105$ cm./sec.

Decay of Air Velocity Along the Spray Axis

The variation of air velocity along the spray axis is determined by taking force and momentum balances across an element of spray as shown in Figure 8, assuming the air velocity distribution within the element to be represented by an average velocity.

By neglecting gravity the force balance on the element may be written as

$$2\,a\,h\,\phi\,dh\,m_1\,u\,\frac{du}{dh} - \frac{d}{dt}\,(m\,v_m) - 2\,R\,h\,\phi\,dh = 0 \tag{21}$$

where v_m the average velocity across the spray is given by

$$v_m = \frac{1}{a - d_0}\int_{d_0}^{a} v\,dx \tag{22}$$

$$= \frac{v_c - v_d}{\beta} \tag{23}$$

since

$$a >> d_0$$

Now

$$\frac{d}{dt}\,(m\,v_m) = v_m\frac{dm}{dt} + m\frac{d\,v_m}{dt} \tag{24}$$

and since for a given element

$$\frac{dm}{dt} + \frac{\partial}{\partial h}\,(2\,a\,h\,\phi\,\rho_a\,v_m)\,dh = 0 \tag{25}$$

therefore

$$\frac{d}{dt}\,(m\,v_m) = -2\,\phi\,\rho_a\,a\,dh\,v_m^2 - 2\,\phi\,\rho_a\,h\,dh\,v_m^2\,\frac{da}{dh} \tag{26}$$

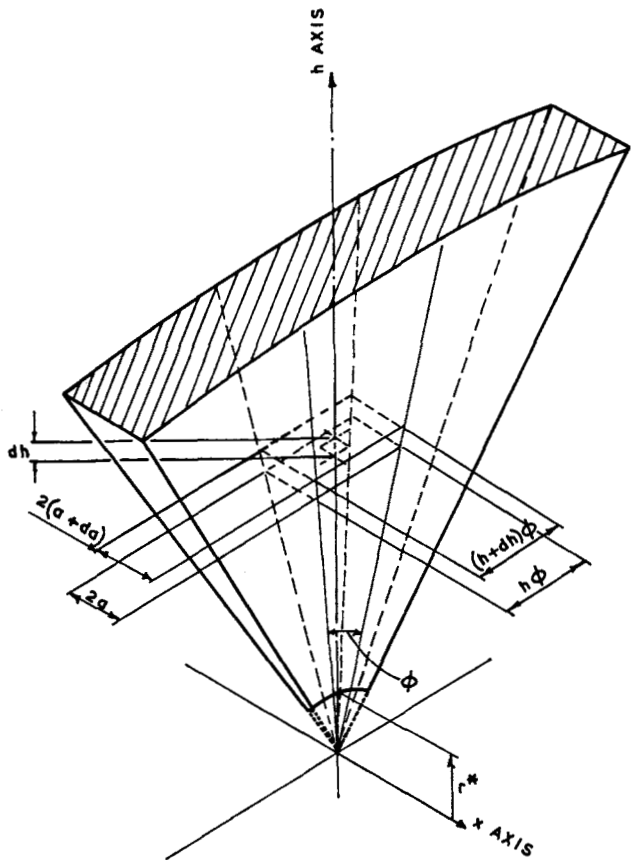

Fig. 8. Sector of spray.

Hence Equation (21) may be rewritten as

$$\frac{m_e}{2h\phi}\frac{du}{dh} = -2\rho_a \cdot K_1 \cdot \left[\frac{v_c - v_d}{\beta} + v_d\right]^2 + \rho_a (v_c - v_d)^2 K^2 \quad (27)$$

taking the further approximation that

$$a = K_1 h \quad (28)$$

At any section the momentum of the liquid is $m_e u$ and the momentum of the air is $2\rho_a h \phi a(v_m + v_d)^2$, so that the total momentum at height h is given by

$$2\rho_a h\phi a (v_m + v_d)v_d + M_o = m_e u + 2\rho_a h\phi a (v_m + v_d)^2$$

where the first term corresponds to the initial momentum of the air around the spray.

When v_d is small compared with $(v_m + v_d)$ little error is incurred in neglecting the first term, and the expression may be rewritten as

$$m_e u + 2\rho_a \phi K_1 h^2\left[\frac{v_c - v_d}{\beta} + v_d\right]^2 - M_o = 0 \quad (29)$$

By differentiating for a given set of operating conditions, that is, for constant m_e, ρ_a, K_1, β and v_d

$$\frac{m_e}{2h\phi}\frac{du}{dh} = -2\rho_a K_1\left[\frac{v_c - v_d}{\beta} + v_d\right]^2 - 2\rho_a K_1 h\left[\frac{v_c - v_d}{\beta} + v_d\right]\frac{1}{\beta}\frac{dv_c}{dh} \quad (30)$$

Equating Equations (27) and (30) and integrating for the boundary conditions $v_c = v_i$ when $h = r^*$ and $v_c = v_c$ when $h = h$, one obtains

$$\frac{\delta^2}{2K_1}\ln\frac{h}{r^*} = \ln\frac{v_i - v_d}{v_c - v_d} + \beta v_d\left[\frac{1}{v_c - v_d} - \frac{1}{v_i - v_d}\right] \quad (31)$$

Since the air in contact with the sheet is moving with the sheet velocity, the initial velocity of the air may be taken as equal to that of the sheet, that is, $v_i = U$.

For $v_d = 0$, Equation (31) reduces to

$$\frac{\delta^2}{2K_1}\ln\frac{h}{r^*} = \ln\frac{U}{v_c} \quad (32)$$

Measured Values

Measurements of the axial air velocity were made up to a height of 12 cm. above the nozzle. At this height the axial air velocity decayed to at least 20% of its original value. The value of K_1 [see Equation (28)] has been obtained by two methods: directly from the photographs of the spray boundary as indicated in Figure 5, and by means of Equation (31) from a plot of

$$\log\frac{v_c - v_d}{U - v_d} - \frac{\beta v_d}{2.3}\left(\frac{1}{v_c - v_d} - \frac{1}{v_i - v_d}\right)$$

against

$$\frac{\delta^2}{2}\log\frac{r^*}{h}$$

for each ejection pressure. The two sets of results are compared in Table 4, where it is seen that except for the lower pressure reasonable agreement exists between measured and derived values. The duct air velocities employed in this work have little effect on K_1, and mean values have been determined in both cases.

Equation (31) is plotted in Figure 9 by using the derived values of K_1 and the experimental results show satisfactory agreement with theory.

For turbulent gas jets the velocity at any height along the axis may be represented by an equation having the form (*19*)

$$\ln\frac{v_i - v_d}{v_c - v_d} = S\ln\frac{h}{h_1} \quad (33)$$

Equation (33) is of similar form to that of Equation (31) apart from the extra term on the right-hand side of Equation (31), which is of significance only when the air velocity along the spray axis is small compared to the ejection velocity, that is, a relatively long distance from the nozzle. The values of S are independent of ejection velocity, being approximately 0.5 for two-dimensional gas jets (*18*) and 1 for three-dimensional jets (*21*). The corresponding parameter $\delta^2/2K_1$ for sprays in air, as given in the last column of Table 4, varies from 3.7 to 0.65. In Equation (33) the axial distance h_1 at which the axial gas velocity begins to depart from the ejection velocity depends on the nozzle diameter and on the ratio of the surrounding air and ejection velocities, and is analogous to the break-up length r^* for sprays.

Table 4. Air Velocity Parameters at Various Ejection Pressures

	P, lb./sq. in.	β	Drop size, microns	K_1, derived	K_1, measured	$\delta^2/2K_1$
Iso-octane	7.6	5.0	40	0.02	0.04	3.7
	22.5	5.9	28	0.04	0.04	1.9
	45.5	6.3	22	0.06	0.08	1.38
	76.8	6.7	19	0.11	0.12	0.75
	118.0	7.0	16	0.12	0.13	0.65
Tetralin	45.5	6.0	25	0.05	—	1.68
	76.8	6.2	21	0.06	—	1.37
	118.0	6.4	18	0.08	0.1	1.05

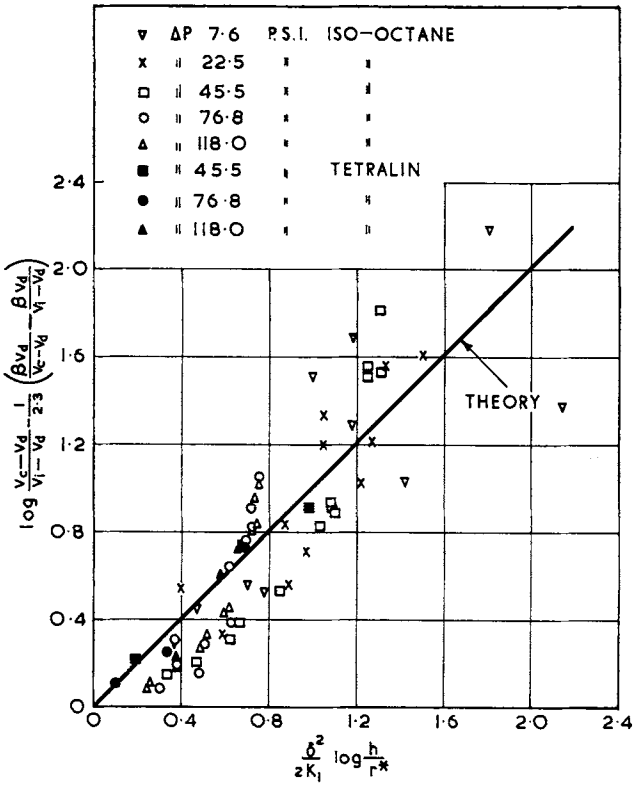

Fig. 9. Decay of air velocity along spray axis for iso-octane and tetralin.

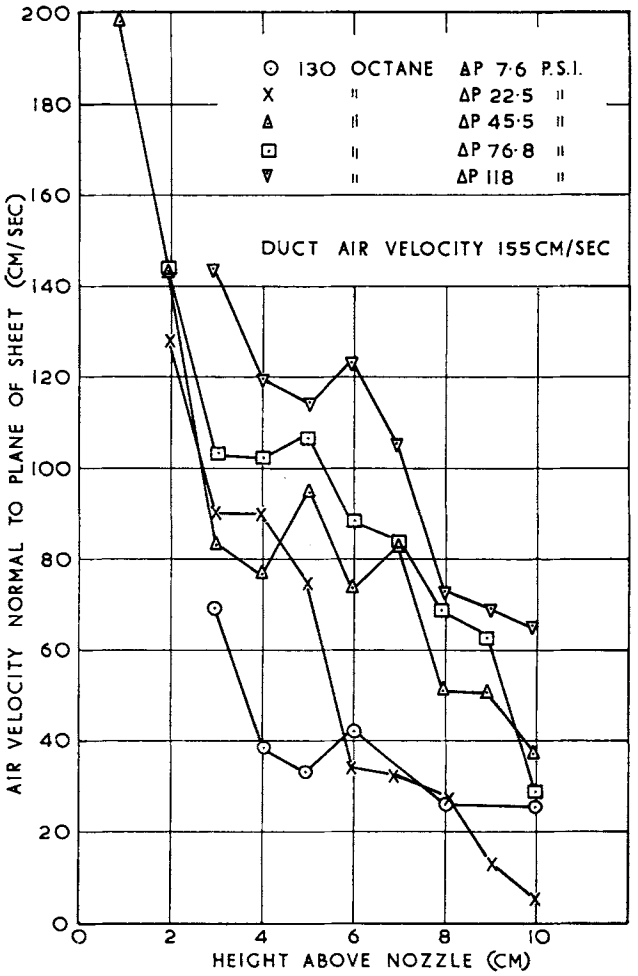

Fig. 10. Air velocity at spray boundary at various heights above nozzle.

Entrainment of Air into the Spray

The theoretical quantity of air entrained up to a given height in the spray is obtained from the product of the average air velocity across the spray and the spray cross-sectional area at that height.

Hence from Equation (23)

$$M_e = 2\,a\,h\,\rho_a\,\phi\left[\frac{v_c - v_d}{\beta}\right] \qquad (34)$$

The total mass of air M passing through the spray is made up of the air entrained by the spray and that forced through it by the surrounding air stream, that is

$$M = 2\,a\,h\,\rho_a\,\phi\,[(v_c - v_d)/\beta + v_d] \qquad (35)$$

The actual amount of air flowing through the spray was determined as follows. The profile of each spray (Figure 4) was divided into segments approximately 0.1 cm. in height up to a distance of 10 cm. from the nozzle. The area of the boundaries at the sides of each segment through which air is passing was then computed. The air flowing into each increment was obtained from the product of the area and the velocity normal to it.

A set of results showing instantaneous values of air velocity normal to the plane of the sheet along the spray boundary is plotted in Figure 10. The curves indicate that air velocity tends to decrease with axial distance from the nozzle. No attempt has been made to draw smooth curves through the points since a study of the photographs (Figure 4) reveals that the apparent scatter is not due to experimental error but from the fact that drops are not uniformly distributed in space but tend to be contained within bands.

A typical set of results giving the cumulative mass of air flowing through a five degree sector around the spray axis ($\phi = 5$ deg.) over a range of ejection pressures is shown in Figure 11. The results are replotted in Figure 12 to show the air-liquid mass ratio M/M_l within the spray

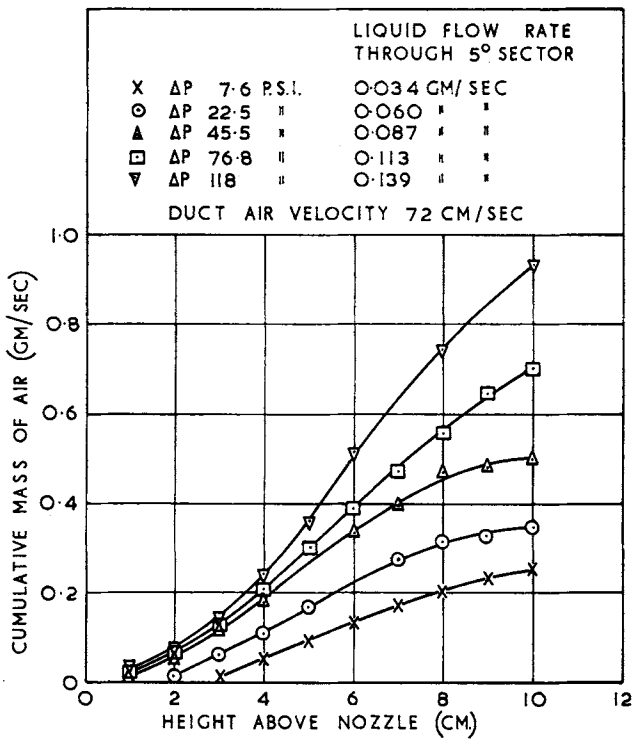

Fig. 11. Cumulative air mass flowing through a 5-deg. sector around the spray axis.

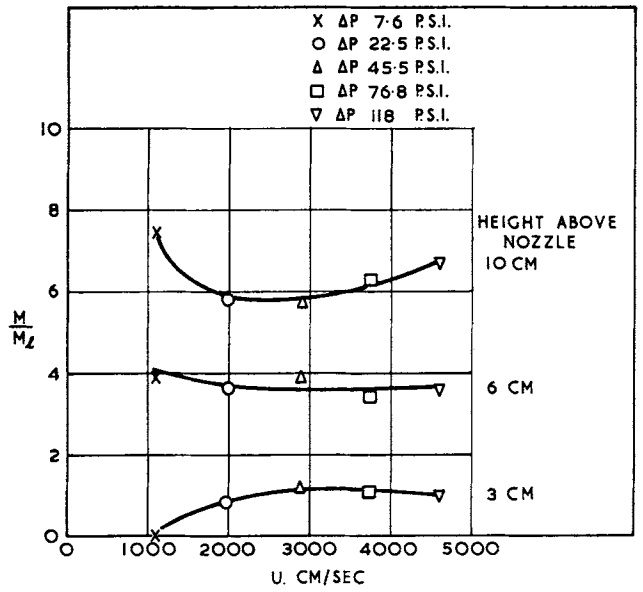

Fig. 12. Variation of M/M_l with liquid ejection velocity at various heights above the nozzle. Iso-octane, duct air velocity, 72 cm./sec.

as a function of ejection velocity U at various heights h above the nozzle. The curves demonstrate that the mass ratio is a complex function of U and h. However, in interpreting these results it must be borne in mind that the break-up length r^* and the spray depth a are each functions of the ejection velocity, so that the spray volume corresponding to any given height h also varies with velocity. More consistent trends are observed in Figure 13 where the results are plotted to show the relation between M/M_l and U at various heights above the region of disintegration of the spray sheet. The figure shows that at any height M/M_l rapidly diminishes with velocity until a value of about 3 to 4,000 cm./sec., after which it tends to a constant value.

The experimental values of M show reasonable agreement with the corresponding values calculated from Equation (35). This is seen in Figure 14, which represents data up to a height of 10 cm.

By expressing M_e as the dimensionless ratio M_e/M_l where

$$M_l = \phi K_o U \rho_l \tag{36}$$

we have from Equations (32) and (34) for $v_d = 0$

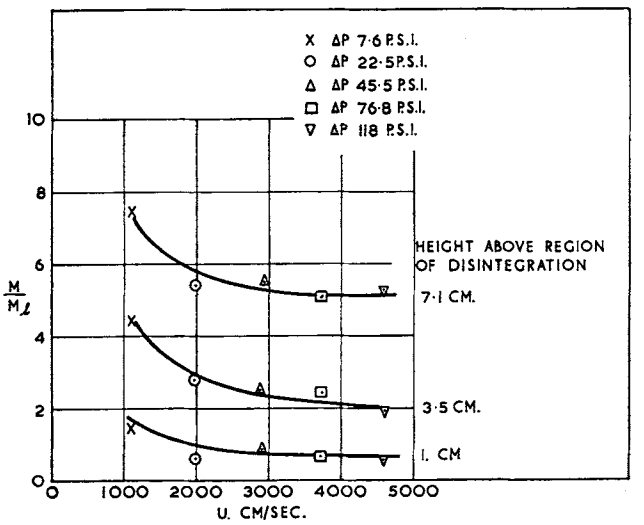

Fig. 13. Variation of M/M_l with ejection velocity at various heights above the region of disintegration. Iso-octane, duct air velocity, 72 cm./sec.

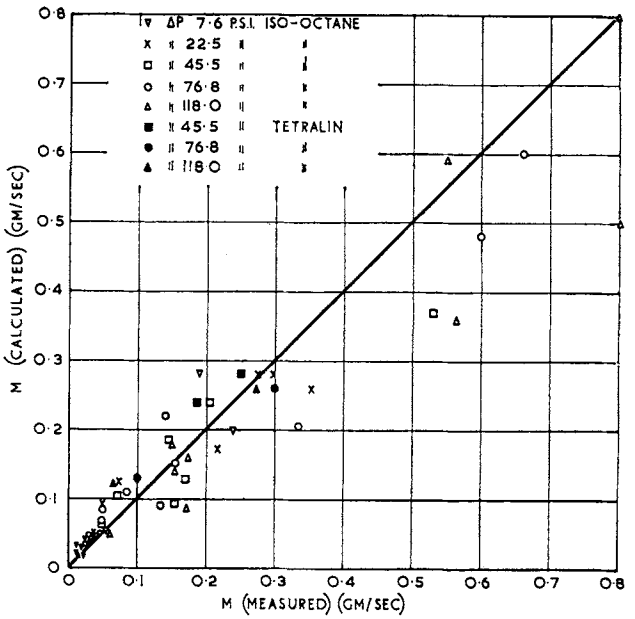

Fig. 14. Comparison of calculated and measured values of air mass flowing through 5-deg. sector of spray.

$$\frac{M_e}{M_l} = \frac{2}{K_o}\frac{\rho_a}{\rho_l}\frac{K_1}{\beta}h^2\left[\frac{r^*}{h}\right]^{\delta^2/2K_1} \tag{37}$$

It can be shown (see Appendix) that the total mass of gas entrained by a turbulent gas jet from a quiescent atmosphere of the same gas is given by

$$\frac{M_e}{M_n} = \frac{8}{D^2}K_2^2 h^2\left[\frac{h_1}{h}\right]^S - 1 \tag{A7}$$

It is difficult to make any direct comparison between Equations (37) and (A7) because of the interrelations of most of the variables in Equation (37) and their dependence upon the liquid ejection velocity. In Equation (A7), h_1 and K_2 are independent of jet velocity, the former being a function of D only. However, it can be seen that the two equations are of similar form, the nozzle parameter K_o corresponding to D^2, K_1/β to K_2^2. r^* to h_1, and the index $\delta^2/2K_1$ to S. In the latter case, S is independent of operating conditions with a value of 1. $\delta^2/2K_1$ varies with operating conditions, although it can be shown that at ejection pressures higher than those used in the present work it tends to a constant value of approximately 0.45 which, it is interesting to note, is close to the value of 0.5 found (*18*) for two-dimensional gas jets.

ACKNOWLEDGMENT

The authors wish to thank R. P. Fraser for valuable advice and the Shell International Co., Ltd., for the provision of a research grant.

NOTATION

(In c.g.s. units unless otherwise stated)

A = thickness of liquid sheet
A^* = thickness of liquid sheet at break-up
a = half spray width in the direction of the x axis as calculated from Equations (17) and (19)
B = dimensionless parameter = $(18\mu/d^2\rho_l)$
C = constant
C_q = coefficient of discharge
D = nozzle diameter
d = drop diameter
d_{10} = number mean drop diameter $(\Sigma nd/\Sigma n)$, microns
d_o = characteristic dimension

E = dimensionless parameter, $\ln x^*/x_o$
e = height of protuberance on flat surface
e_{crit} = critical height of protuberance
g = acceleration due to gravity
h = distance along spray axis from nozzle
h_1 = distance at which axial velocity begins to depart from the injection velocity
K^2 = friction factor
K_o = nozzle parameter = rA
K_1 = constant = ah
K_2 = constant
l = distance along plate or from region of liquid sheet disintegration
M = mass of air flowing through spray
M_e = mass of entrained air
M_l = liquid flow rate
M_n = air mass flowing through nozzle
M_o = initial momentum of drops
M_t = total mass of gas flowing through gas jet
m = mass of air within element of spray
m_e = liquid mass flow rate through element
m_l = mass of liquid per unit volume of spray = $m_e/(2\,a\,h\,\phi\,U)$
N_{We} = Weber number $(\rho_l\,U^2A^*/2\gamma)$
n = number of drops with diameter d
ΔP = pressure differential, lb./sq.in.
R = shear stress
r = length of liquid sheet
r^* = break-up length of liquid sheet
r_m^* = measured length of liquid sheet
r_t^* = calculated length of liquid sheet
S = dimensionless parameter ($\delta^2/2K_1$ for sprays)
t = time
U = liquid ejection velocity
U_j = gas ejection velocity
U_p = gas velocity relative to flat plate
u = drop velocity
u_n = initial normal velocity component of drop
u_r = initial radial velocity component of drop
V_c = gas velocity along jet axis
v = air velocity in direction of h axis or gas jet axis
v_c = air velocity within spray along plane of sheet
v_d = air velocity in duct
v_i = initial air velocity
v_m = average air velocity
x = distance normal to spray or gas jet axis
x' = wave amplitude after time t
x^* = wave amplitude at instant of disintegration
x_o = initial wave amplitude

Greek Letters

α = growth rate of waves
β = dimensionless parameter = K/δ
γ = surface tension
δ = constant
ϕ = included angle of element of spray
μ = gas viscosity
ρ_a = density of ambient gas
ρ_l = liquid density
ρ_j = gas jet density
σ = spreading coefficient defined in reference 21
θ = maximum angle at which drops are ejected out of the plane of sheet (see Figure 3)

LITERATURE CITED

1. Binark, H., and W. E. Ranz, *Am. Soc. Mech. Engrs. Preprint* 58-A-284 (1959).
2. Gluckert, F. A., *A.I.Ch.E. J.*, **8**, 460 (1962).
3. Rasbash, D. J., and G. W. V. Stark, *Chem. Eng.*, 164 (1962).
4. Dorman, R. G., *Brit. J. Appl. Phys.*, **3**, 189 (1952).
5. Dombrowski, Norman, and R. P. Fraser, *Phil. Trans. Roy. Soc.*, **A247**, 101 (1954).
6. Dombrowski, Norman, David Hasson, and D. E. Ward, *Chem. Eng. Sci.*, **12**, 35 (1960).
7. ———, *J. Agric. Eng. Res.*, **6**, 37 (1961).
8. Hasson, David, and J. Misrahi, *Trans. Inst. Chem. Engrs.*, **39**, 415 (1961).
9. Dombrowski, Norman, and P. C. Hooper, *Chem. Eng. Sci.*, **17**, 291 (1962).
10. Fraser, R. P., Paul Eisenklam, Norman Dombrowski, and David Hasson, *A.I.Ch.E. J.*, **8**, 672 (1962).
11. Dombrowski, Norman, and W. R. Johns, *Chem. Eng. Sci.*, **18**, 203 (1963).
12. Whitehead, L. G., L. Y. Wu, and M. H. L. Waters, *Aeronaut. Quart.*, **2**, 254 (1951).
13. Gregory, P. H., *Ann. Appl. Biol.*, **38**, 357 (1951).
14. Timmermans, Jean, "Physico-Chemical Constants of Pure Organic Compounds," Elsevier, New York (1950).
15. Squire, H. B., *Brit. J. Appl. Phys.*, **4**, 167 (1953).
16. Coulson, J. M., and J. F. Richardson, "Chemical Engineering," Pergamon Press, London (1957).
17. Prandtl, L., "Essentials of Fluid-Dynamics," Blackie & Son, Ltd., London (1953).
18. Schlichting, Hermann, "Boundary Layer Theory," Pergamon Press, London (1955).
19. Spalding, D. B., "Combustion and Propulsion," 3 AGARD Colloquium, p. 269, Pergamon Press, London (1959).
20. Ricou, F., and D. B. Spalding, *J. Fluid Mech.*, **11**, 21 (1961).
21. Albertson, M. N., Y. B. Dai, R. A. Jensen, and Hunter Rouse, *Proc. Am. Soc. Civ. Engrs.*, **74**, 1571 (1948).

APPENDIX: AIR ENTRAINMENT INTO A TURBULENT GAS JET

The total quantity of gas flowing through any section normal to the axis of a circular gas jet in an atmosphere of the same gas is

$$M_t = 2\pi\rho_j \int_o^\infty v\,x\,dx \qquad (A.1)$$

Albertson et al. (*21*) have shown that the velocity profile across a turbulent circular jet in a quiescent atmosphere is given by

$$\frac{v}{V_c} = \exp -(x^2/2\,\sigma^2) \qquad (A.2)$$

Thus combining Equations (A.1) and (A.2) and integrating, one obtains

$$M_t = 2\,\pi\,\rho_j\,v_c\,\sigma^2 \qquad (A.3)$$

σ^2 may be expressed in terms of h, the height above the nozzle, by

$$\sigma = K_2 h \qquad (A.4)$$

so that Equation (A.3) may be rewritten as

$$M_t = 2\,\pi\,\rho_j\,v_i\,K_2^2\,h^2\left(\frac{h_i}{h}\right)^S \qquad (A.5)$$

The mass flow rate through the nozzle is

$$M_n = \pi\frac{D^2}{4}\rho_j\,U_j \qquad (A.6)$$

Thus the entrained mass of gas per unit flow through the nozzle is

$$\frac{M_t - M_n}{M_n} = \frac{M_e}{M_n} = \frac{8}{D^2}K_2^2\,h^2\left[\frac{h_1}{h}\right]^S - 1 \qquad (A.7)$$

Albertson et al. have found that K_2 has a value of 0.081, $h_1 = 6.2\,D$, and that S is equal to 1.

Equation (A.7) may thus be simplified to give

$$M_e/M_n = 0.327\,h/D - 1 \qquad (A.8)$$

Equation (A.8) compares favorably with the semiempirical relation of Ricou and Spalding (*20*):

$$M_e/M_n = 0.32\,h/D - 1 \qquad (A.9)$$

Manuscript received August 3, 1965; revision received February 8, 1966; paper accepted February 9, 1966.